Turkish Journal of Electrical Engineering & Computer Sciences

http://journals.tubitak.gov.tr/elektrik/

Research Article

Turk J Elec Eng & Comp Sci
(2017) 25: 3798 – 3810

doi:10.3906/elk-1606-343

Using the variable width in a planar inductor on Kapton for optimizing its performance

Hayet KHARBOUCH[1,*], Azzedine HAMID[1], Thierry LEBEY[2], Vincent BLEY[2], Léon HAVEZ[2], Celine COMBETTE[2]

[1]Department of Electrical Engineering, Faculty of Electrical Engineering, University of Sciences and Technology of Oran, Oran, Algeria

[2]Paul Sabatier University, Toulouse, France

Received: 21.06.2016 • **Accepted/Published Online:** 25.02.2017 • **Final Version:** 05.10.2017

Abstract: In this paper, we examine the design of planar inductors and consider an expansion of the conductor to reduce its resistance. An increase in the number of turns increases the proximity effect, capacitive coupling, and skin effect. The resulting effect will translate into an increase in the area occupied by the inductor and a decrease in the inductors' performances. In order to solve such difficulties, an alternative approach is to design tapered inductors. For the same electrical and geometrical characteristics, a tapered inductor occupies a larger area than a standard inductor. Our approach consists of designing a new concept regarding tapered planar inductors that occupy the same surface and maintain the same electrical characteristics as the standard planar inductor regarding the following topologies: circular, hexagonal, and square. The results obtained show that impedance is more important in the case of the tapered inductor. Higher impedance implies smaller current and hence smaller parasitic effects of the capacitance series and proximity effect.

Key words: Passive components, integration, tapered planar inductor, ferrite

1. Introduction

Nowadays, miniaturization of active and passive electronic components has become a wide research area [1]. It is an increasing trend to manufacture electronic equipment and accessories that represent high consumer products such as hard drives, mobile phones, and automotive industry such as avionics and ships. The aim of this interest in miniaturization is, on the one hand, to increase the number of functionalities on the same chip and, on the other hand, to reduce the cost by putting in place a system of mass production [2,3]. In a number of cases, hybrid systems offer facilities for volume reduction. However, passive components represent a holdback to miniaturization. Nowadays, inductance is a key component in the electronics arena and represents an important factor for its progress. Several models have been considered to improve its characteristics [4–7]. The model of tapered inductors improves the performance of the planar inductor. Indeed, in this specific model, we need to change the conductor's width in order to reduce its resistance [8,9]. For a standard inductor in the absence of a magnetic circuit, the concentration of the magnetic field at the centre of the inductor generates a worse distribution of the current within the central inductor than for the peripheral inductor. For a tapered inductor, the distribution of the current in each turn of the spiral is homogeneous. This makes it possible to exploit the copper section optimally. It is evident that the current density is higher for the inner turns

*Correspondence: hayet.kharbouch@gmail.com

than for the outer turns, which could cause greater heating in the center; however, the resistance of each turn remains in accordance with the desired design [10]. In this work, we will focus on the design, manufacture, and characterization of planar inductor spirals on a magnetic layer. We consider two types of inductors: standard and tapered inductors. The second type of inductor is characterized by an increasing track width according to the radius. This approach is of particular interest to the inductor, as the total DC resistance will be effectively reduced to a given number of turns. Indeed, on the one hand, this will compensate for the variation of the resistance linked to the increase in conductor width of the inductor [11]. On the other hand, it will reduce the proximity and capacitive effects between turns. The gain is less perceptible because we have considered the same occupied space for all prototypes of inductors studied. This study has targeted the following topologies: circular, square, and hexagonal, which are represented in Figure 1. The parameters that have been taken into account in this study are topology, turns' width, interturn distance, and thickness of the conductor [12,13]. The production and characterization took place in the Laboratory on Plasma and Conversion of Energy-UMR5213, Team MDCE, Toulouse, France.

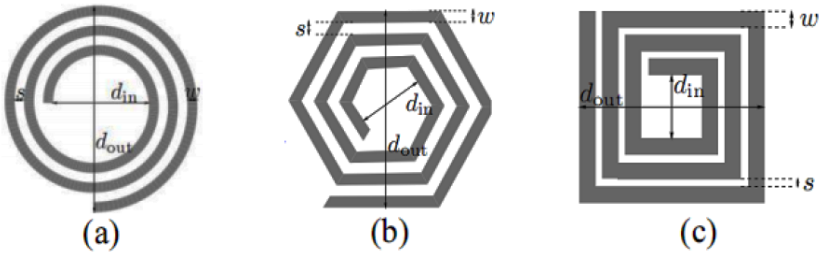

Figure 1. Different studied topologies: (a) circular, (b) hexagonal, and (c) square.

2. Characteristics of planar inductors

In this section, we present the geometrical and electrical characteristics of standard and tapered inductors.

2.1. Geometrical parameters

In Figure 2, we present a 3D representation of planar inductors made in this study. Our strategy is to keep the same area occupied by the inductors and calculate the electrical parameters in particular values of the series inductance and resistance. The various stages of implementation are detailed in Section 3.

For a given shape, an inductor is specified by the number of turns n, turn width w, turn spacing s, thickness t of the conductor, total conductor length l_t, average diameter d_{avg}, outer and inner diameters d_{out} and d_{in}, as shown in Figure 1 [14]. The dimensions of the different topologies are as follows: d_{out}= 10 mm, d_{in}= 1 mm, and $n = 3$. For a tapered inductor, $w1$, $w2$, and $w3$ are the widths of winding of each turn, as shown in Figure 2.

The results of geometric parameters included in Table 1 are obtained for conductor material copper (Cu) and magnetic material N87.

We note that the total lengths vary according to the topology. The square spiral has the largest value, the smallest circular spiral, hence the interest in calculating the value of the resistance for each topology. The total length of the inductor can be expressed as

$$l_t = n d_{avg} N \tan(\pi/N) \quad (1)$$

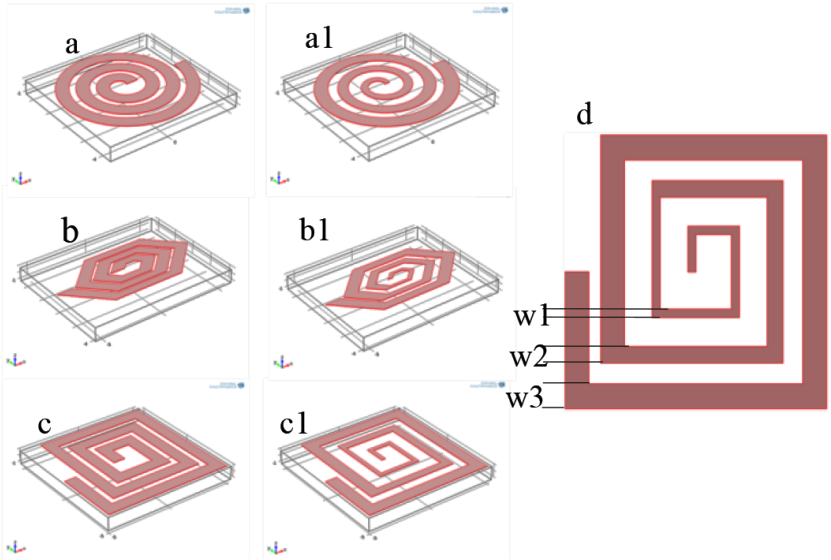

Figure 2. 3D representation of planar inductors realized circular, hexagonal, and square.

Table 1. Geometric parameters for standard and tapered inductors.

			Tapered inductors	Standard inductors
Topology	l_t (cm)	$t\,(\mu m)$	$w1/w2/w3$ (mm)	w (mm)
Circular	4.7	35	0.3/ 0.6/ 0.9	0.9
Hexagonal	5.2	35	0.3/0.6/ 0.9	0.9
Square	6.0	35	0.3 /0.6/0.9	0.9

For a square inductor, $N = 4$ and for a hexagonal inductor, $N = 6$. N is a big number for the circular inductor, where we get the expressions of the total length l_t Eq. (2) [15].

$$l_t = \pi N d_{avg} \tag{2}$$

$$d_{avg} = \frac{d_{out} + d_{in}}{2} \tag{3}$$

2.2. Simplified physical model of a inductor on ferrite

The model includes the series inductance L_s, series resistance R_s, coupling capacitance between the turns C_s, capacitance associated with the insulation layer (Kapton) with the substrate C_k, capacity substrate C_{sub}, and resistance associated with substrate R_{sub}. The equivalent electrical model of the integrated microinductor [16] is shown in Figure 3. Inductance L_s is calculated by Mohan's formula, expressed by Eq. (4) [17].

$$L_s = \frac{\mu_0 n^2 d_{avg} c_1}{2} \left(\ln\left(\frac{c_2}{\rho}\right) + c_3 + c_4 \right) \tag{4}$$

$$\rho = \frac{d_{out} - d_{in}}{d_{out} + d_{in}} \tag{5}$$

Coefficients c_1, c_2, c_3 and c_4 are defined for each geometry as given in Table 2.

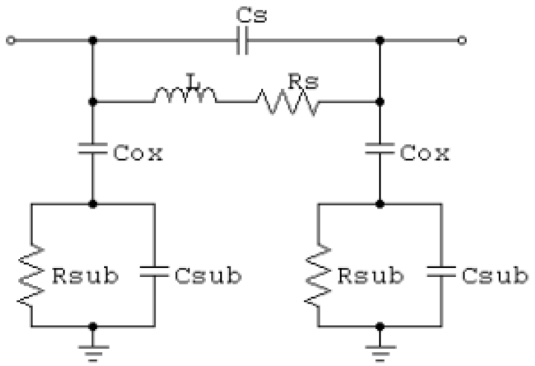

Figure 3. Equivalent model of a planar inductor [18].

Table 2. Parameter values of c [17].

Geometry	c_1	c_2	c_3	c_4
Square	1.27	2.07	0.18	0.13
Hexagonal	1.09	2.23	0	0.17
Circular	1	2.46	0	0.2

With:

$$R_s = \frac{\rho l_t}{S_c} = \frac{\rho l_t}{wt} \tag{6}$$

$$d_{out} = d_{in} + 2\left(nw + (n-1)\, s\right) \tag{7}$$

ρ : resistivity of copper, S_c : section of the conductor, s : interturns spacing.

2.3. Electrical parameters

The calculation of electrical parameters, especially series resistance R_s and series inductance L_s, obtained by the implementation of Mohan's formula, show the importance of topology. The results of electrical dimensioning for the three topologies are shown in Table 3.

Table 3. Electrical parameters of standard and tapered planar spiral inductors.

		Standard inductors			Tapered inductors		
		Square	Hexagonal	Circular	Square	Hexagonal	Circular
$R_s\,(m\Omega)$		36.8	35	28.5	55.2	51	43.7
$L_s(nH)$	In air	49.49	45.06	40.053	49.49	45.06	40.05
	With N87	74.23	67.59	60.07	74.23	67.59	60.07
L_s/R_s		$2.02.10^{-6}$	$1.93.10^{-6}$	$2.1.10^{-6}$	$1.34.10^{-6}$	$1.32.10^{-6}$	$1.37.10^{-6}$

3. Fabrication process

The planar inductor consists of a copper conductor on a patch of Kapton, all deposited on a ferrite substrate [9,19]. Fabrication was carried out in the Laplace laboratory [20]. Each step was studied and optimized to ensure the performance and reproducibility of the process, as shown in Figure 4.

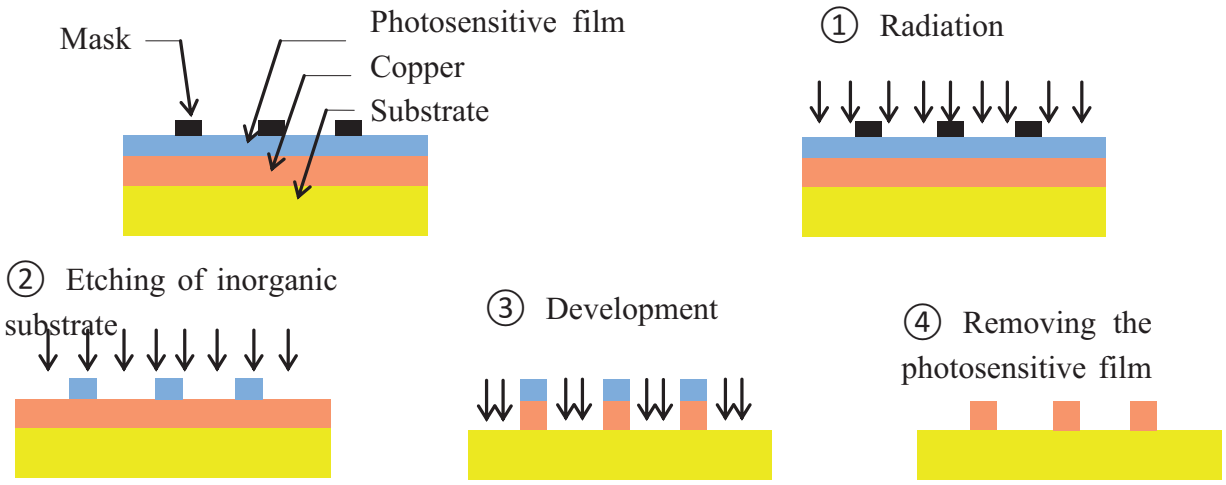

Figure 4. Steps of photolithography.

Firstly, we prepare the magnetic cores N87 by using a chainsaw, shown in Figure 5, to cut $15 \times 15 \times 2$ mm^3 of size. The copper conductors, of $35\mu m$ thickness, are then assembled on these ceramic substrates. The magnetic core serves as a mechanical support for a polyimide film constituted of Kapton and copper, called flex. Then we realize the copper circuits on the flex for the different topologies shown in Figure 2.

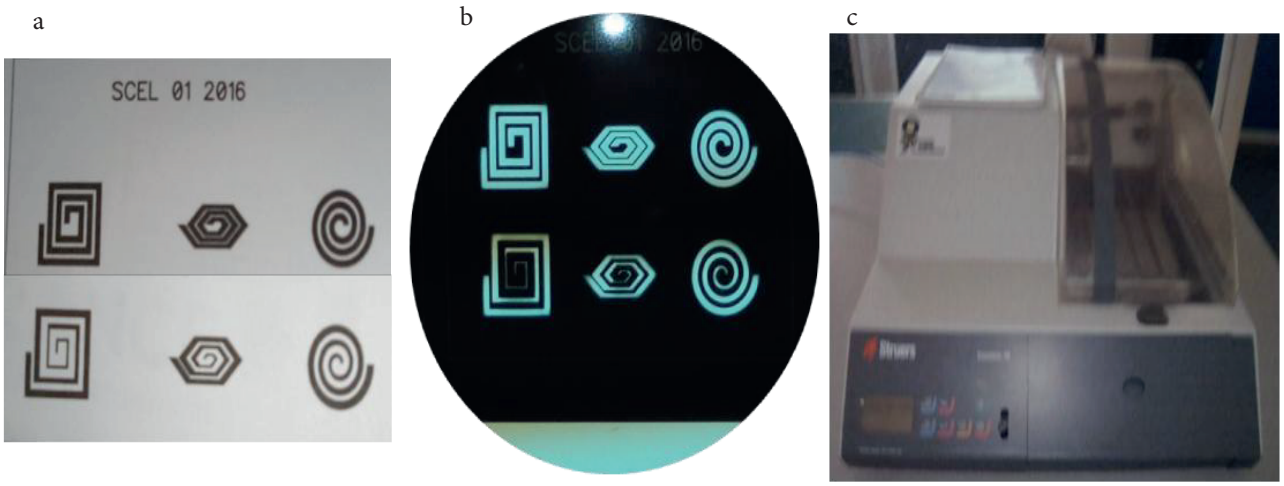

Figure 5. Mask of the prototypes to be realized: (a) printed on paper, (b) printed on transparent paper, and (c) chainsaw (Secotom 10 – STRURES) with a disc.

Next, we present the set of steps for preparing the metallized and masked inorganic substrate. Figure 5 shows the pattern that allows the realization of the mask to etch.

Afterwards, the pattern is engraved on a glass plate covered with a layer of chrome to obtain the mask. The mask is transferred to the flex made of Kapton and $35\mu m$ of copper, called photolithography. The etching allows removing the copper from the surface of the flex. We used wet etching, which involves soaking the sample in a solution composed of iron perchloride and water that is heated to 27 °C. The solution engraves the copper by dissolving the copper that is unprotected by the hardened film, and shows the desired pattern. The final sample is rinsed with water and immersed in a solvent acetone or sodium hydroxide NaOH to remove the blue

film and show the conductive lines. After rinsing, the final component is thus obtained and passed into a 70 °C furnace to avoid oxidation.

Finally, the inductors are varnished to prevent oxidation of the copper conductor. The installation of bonding is essential for the interconnection of the central plot to the outside plot. The topologies carried out are presented in Figures 6a and 6b.

Figure 6. System of chemical etching (left) and topologies realized (right): (a) standards, (b) tapered.

4. Experimental results of prototypes

The characterization of prototypes realized requires both the measurement means adapted and a model to take into account the major physical phenomena. Planar inductors are characterized using LRC meter 4194A. To characterize the inductors without a magnetic core, we realized the conductor on Kapton. We compensated the bonding resistance in order to obtain the accurate value of the series resistance spirals. The measuring bench available at the Laplace laboratory to measure the amplitude and phase signals is presented in Figure 7.

4.1. Choice of equivalent circuit model

The measurement model is chosen by the apparatus and for each specified range according to preset impedance values. In our case, the inductance values to be measured are of the order of several nH [20]. To this effect, we chose the model of the equivalent circuit, indicated in Figure 7, to take measures. The different parameters of the equivalent circuit depend on the frequency.

Inductance L_s, as a function of frequency, enables us to see the influence of the frequency on the inductance value and reports the evolution of the permeability as a function of frequency. Resistance R_s, depending on frequency, takes into account all losses in the conductors. C_s models the capacitive coupling between the turns of the inductor. An optimization algorithm was used to extract the values of the model elements.

4.2. Measurement results for standard planar inductors

The results of the measures of the standard planar inductors for the topologies realized are shown in Table 4.

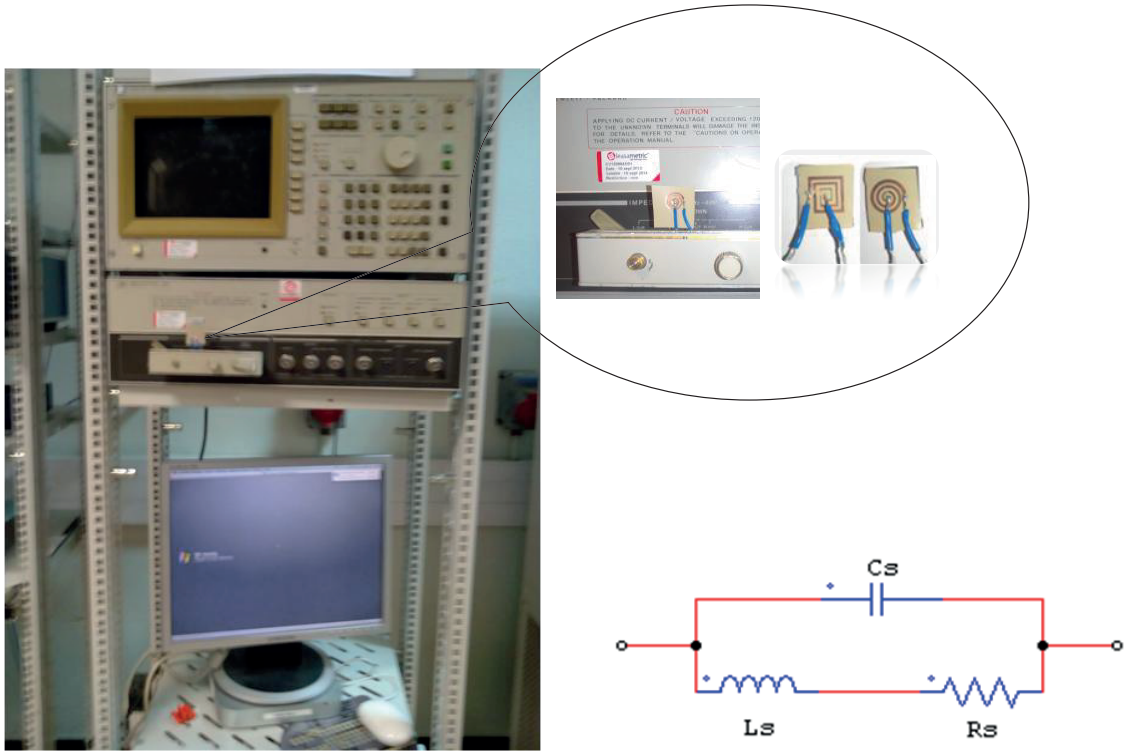

Figure 7. Bank of characterization (left) and equivalent circuit model (right).

Table 4. Results of measures for standard planar inductors.

Values		Standard inductors		
		Square	Hexagonal	Circular
$R_s\,(m\Omega)$		36.14	27	19.56
$L_s\,(nH)$	In air	33.78	13	21.38
	With N87	51.54	12.78	35.64
L_s/R_s		$1.43.10^{-6}$	$0.47.10^{-6}$	$1.82.10^{-6}$

4.3. Measurement results for tapered planar inductors

The results of the measures of the tapered planar inductors for the topologies realized are shown in Table 5.

Table 5. Results of measures for tapered planar inductors.

Values		Tapered inductors		
		Square	Hexagonal	Circular
$lR_{ls}l\,(m\Omega)$		54.59	31.21	32.7
$lL_{ls}l(nH)$	In air	12.98	23.58	21.38
	With N87	13	36.16	35.64
lL_{ls}/lR_{ls}		$1.43.10^{-6}$	$1.43.10^{-6}$	$1.43.10^{-6}$

4.4. Inductive and resistive behavior of inductors

In this paragraph, we present the influence of the magnetic core on the resistive and inductive behavior of the prototypes realized. Figure 8 shows the influence of the frequency on the inductor. For different topologies realized, we note that the inductance of the spiral increases with increasing frequency.

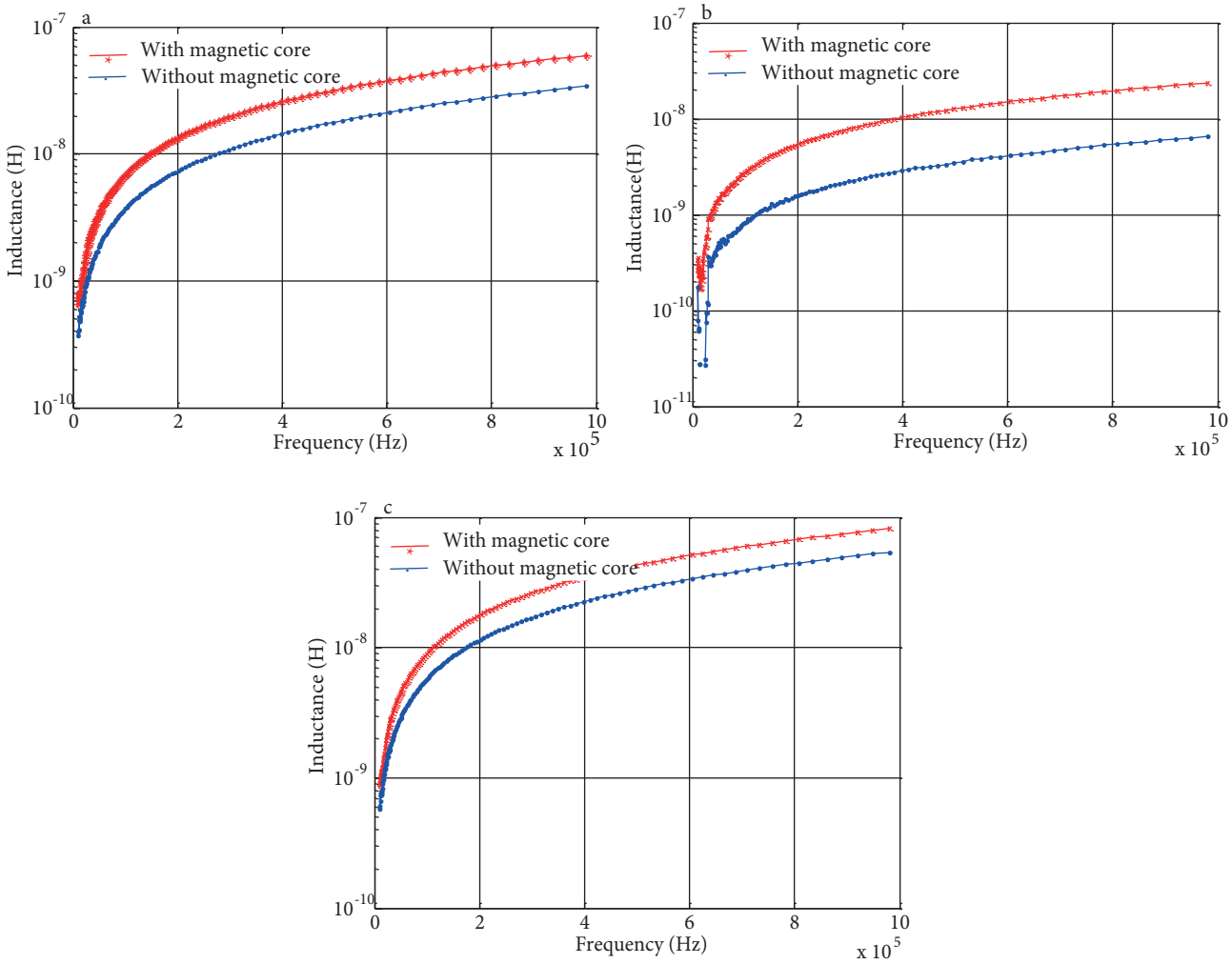

Figure 8. Variation in series inductance depending on the frequency with and without magnetic core for standard inductors: (a) circular, (b) hexagonal, and (c) square.

The value of the inductance has become more important with the use of a magnetic core, because it allows canalizing the lines of the magnetic fields.

Figure 9 shows the influence of the frequency on the resistive behavior for the different topologies realized. We note that the resistance of the spiral increases with increasing frequency.

The resistance of the inductor without the magnetic core is substantially constant, although account must be taken of the skin effect. In this case, the useful section of the conductor decreases with frequency. Therefore, the measured resistance of the inductor with magnetic core increases significantly with frequency.

5. Influence of topology on inductive behavior for standard inductors

The effect of total length is shown in Figures 10 and 11. It varies according to the topology on the resistive and inductive behavior of the realized inductors.

The maximum value of inductance corresponds to the square topology and the minimum value to the circular topology. The intermediate value corresponds to the hexagonal topology, as shown in Figure 10a.

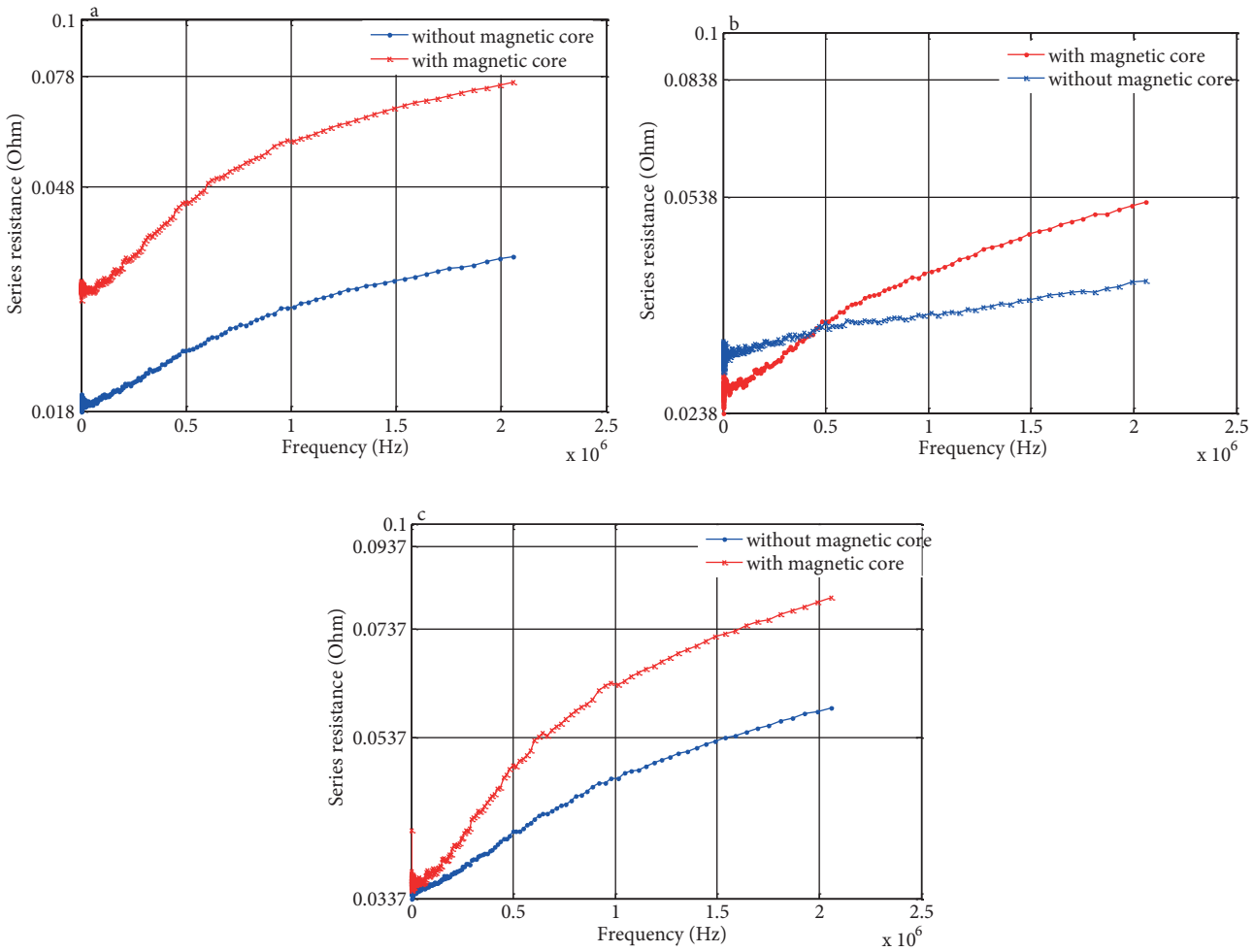

Figure 9. Variation in series resistance depending on the frequency with and without a magnetic core for standard inductors: (a) circular, (b) hexagonal, and (c) square.

We observe in Figure 10b that the maximum value of resistance corresponds to the square topology and the minimum value to the circular topology. The intermediate value corresponds to the hexagonal topology.

Figure 11 allows us to note that the circular topology has the best X/R_s as a function of frequency. This is due to its low resistance compared to hexagonal and square topologies.

5.1. Influence of topology on inductive behavior for tapered inductors

Figure 12 shows the variation of the ratio X/R_s as a function of frequency for the circular, hexagonal, and square tapered inductors.

We find that the circular topology has the best X/R_s as a function of frequency. As in the case of standard inductors, this is also explained by its low resistance compared to hexagonal and square topologies.

6. Behavior in operating mode of prototypes

In this section, we present the frequency behavior of the standard and tapered circular inductors. Figure 13 shows a comparison of inductance values with standard and tapered circular inductors.

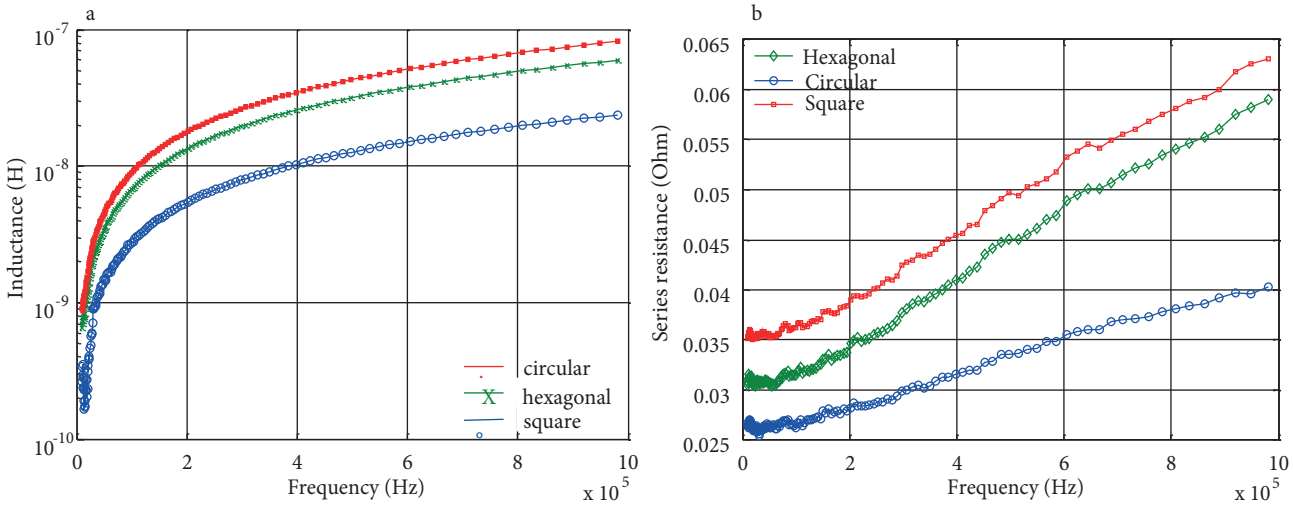

Figure 10. Variation in (a) inductance and (b) series resistance, depending on the frequency for standard inductors.

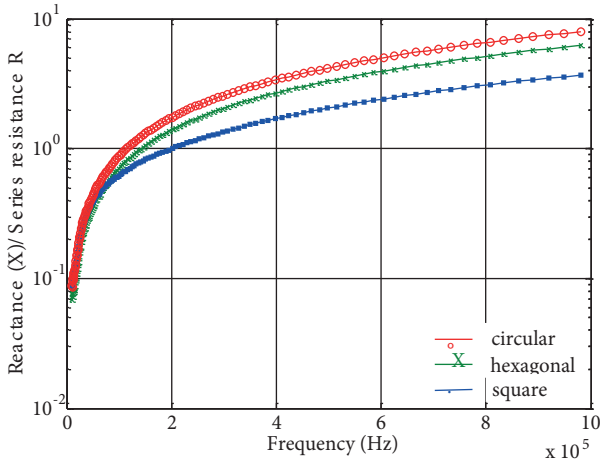

Figure 11. Variation in lX/lR_{ls}, depending on the frequency for standard inductors.

We observe that the value of inductance of the standard and tapered inductors evolves in the same way, depending on the frequency.

Figure 14 illustrates the evaluation of impedance versus frequency of standard and tapered inductors.

We note that impedance is more important in the case of the tapered inductor. Higher impedance implies smaller current and hence smaller parasitic effects of the series capacitance and proximity effect. This is why a tapered inductor presents the best behavior.

Figure 15 shows, by way of example, the variation in the impedance and the phase as a function of the frequency for a tapered planar circular inductor.

It can be seen from these curves that the realized components show resistive behavior up to 10 kHz and inductive beyond 10 kHz. This means that the prototypes made are purely inductive. This reasoning is valid for all inductors made.

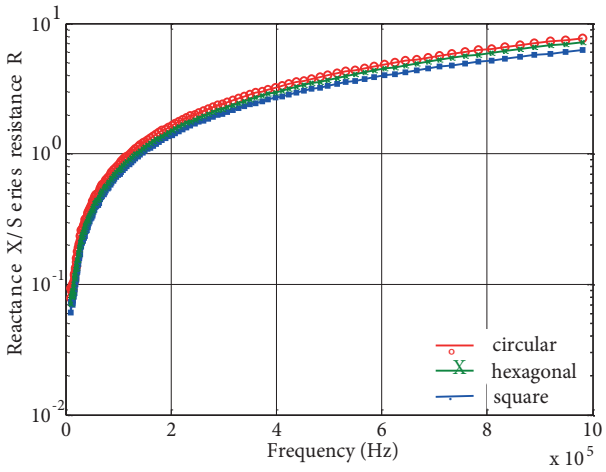

Figure 12. Variation in lX/lR_{ls}, depending on the frequency for tapered inductors.

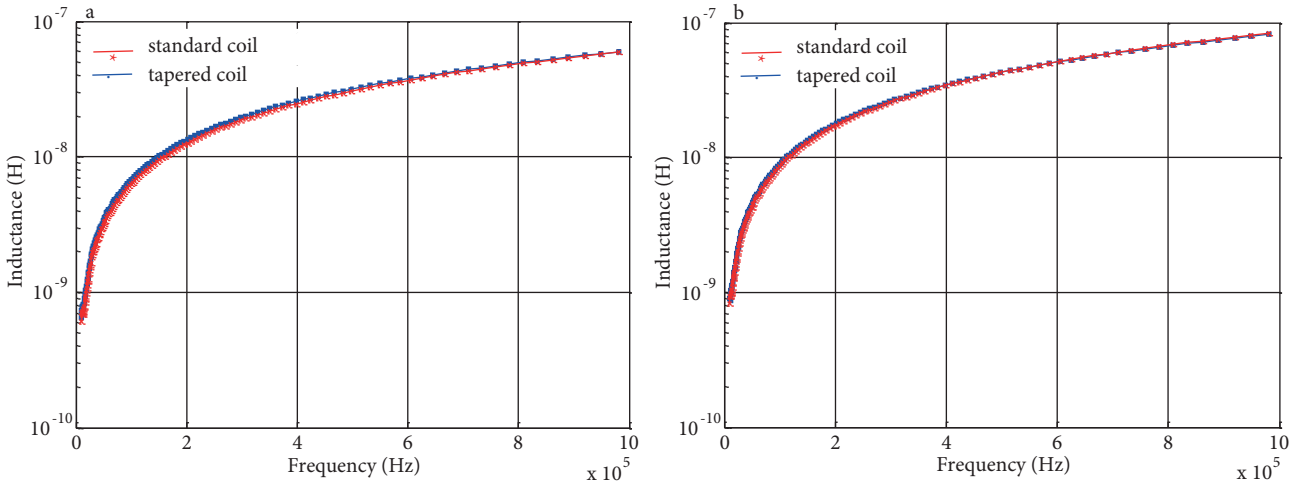

Figure 13. Variation in series inductance depending on the frequency: (a) circular, and (b) square.

7. Conclusion

The work presented in this paper concerns the design, realization, and characterization of standard and tapered inductors. We retained circular, hexagonal, and square topologies. The particularity of the model of the tapered coil is that it allows improvement in the performances of the planar inductor. Indeed, it makes it possible to maintain the same value of inductance while reducing the effect of proximity and the parasitic effects of the series capacitance. The geometrical and electrical dimensioning of these inductors is an important step that requires taking into account many parameters and compromises their manufacture and use. The manufacturing of these inductors was carried out at the Laplace laboratory in Toulouse, France. The use of low-cost commercial ferrite substrates makes it possible to meet a very large number of applications, extending from a few tens of kHz to several hundreds of MHz. The conductive spirals of all prototypes were made on Kapton and on the magnetic material N87. The results obtained show that the magnetic core increases the value of the inductance; both types of inductors, standard and tapered, have the same electrical characteristics while occupying the same area. The inductance of the spiral increases with frequency, and this applies to all inductors. The maximum value of inductance is obtained with square topology and the minimum value with circular topology; this is due

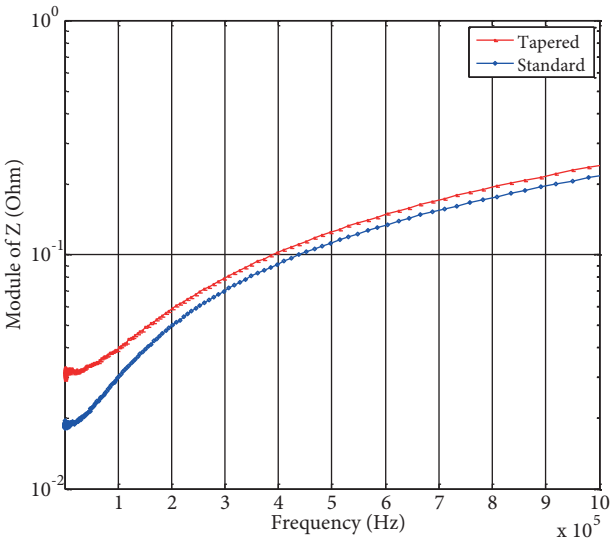

Figure 14. Evolution of impedance depending on the frequency for standard and tapered planar inductors.

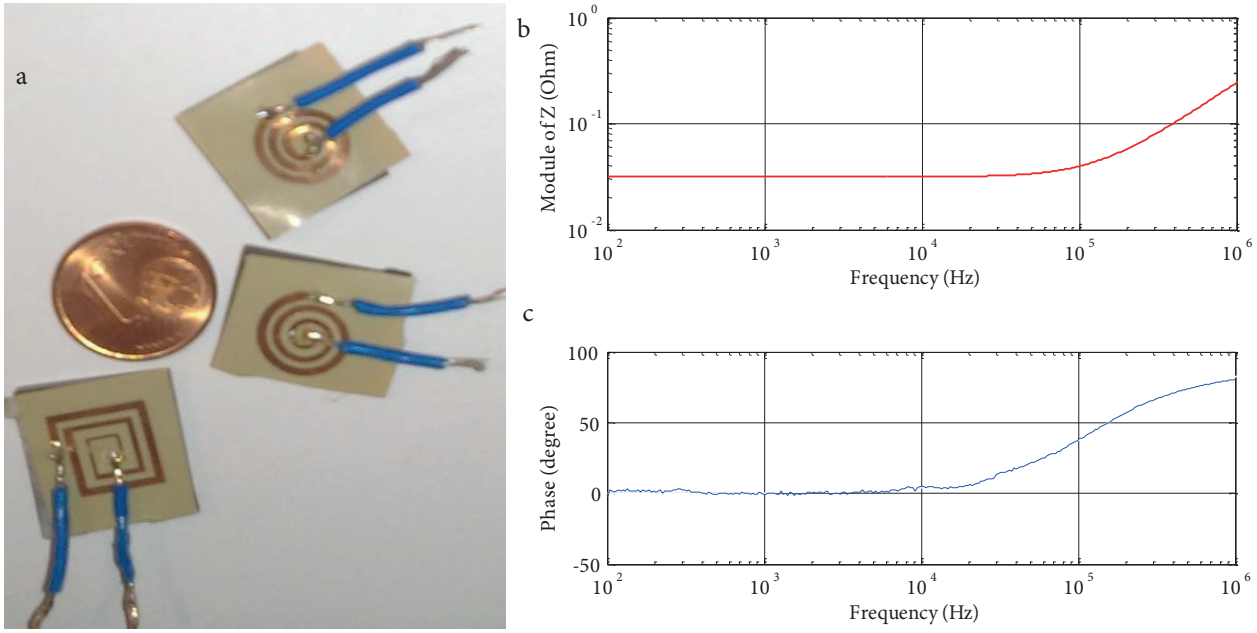

Figure 15. Planar spiral inductors on Kapton and ferrite substrate: (a) impedance, (b) magnitude, and (c) phase, depending on the frequency.

to the geometric specifications of each topology. The electrical resistance of the square inductor is larger than that of the circular inductor for the case of standard and tapered inductors. Indeed, the total length of the conductor of the square inductor is greater than that of the conductor of the circular inductor. The circular topology has the best X/R_s ratio; the inductance of the standard and tapered inductors evolves identically as a function of frequency. The impedance is greater in the case of variable width inductor and so a low-value current will flow, implying a decrease in the parasitic effects of the series capacitance and proximity effect.

References

[1] Melati R, Hamid A, Lebey T, Derkaoui M. Design of a new electrical model of a ferromagnetic planar inductor for its integration in a micro converter. Math Comput Model 2013; 57: 200-227.

[2] Guettaf Y, Rizouga M, Hamid A. Design and modeling of a square planar inductor for a push pull Converter. J Elec Electron Eng Res 2015; 8: 17-22.

[3] Martin C, Allard B, Tournier D, Soueidan M, Rousseau JJ, Allessem D, Menager L, Bley V, Lembeye JY. Planar inductors for high frequency DC-DC converters using microwave magnetic material. In IEEE 2009 Energy Conversion Congress and Exposition Conference; 20–24 September 2009; San Jose, CA, USA. New York, NY, USA: IEEE. pp. 1890-1894.

[4] Derkaoui M, Hamid A, Lebey T, Melati R. Design and modeling of an integrated micro-transformer in a fly back converter. Telkomnika 2013; 11: 669-682.

[5] Estibals B, Salles A. Design and realisation of integrated inductor with low DC-resistance value for integrated power applications. HAIT J Sci Eng B 2005; 2: 848-868.

[6] Kowase I, Sato T, Yamasawa K, Miura Y. A Planar inductor using Mn-Zn ferrite/polyimide composite thick film for low-voltage and large-current DC-DC converter. In: IEEE 2005 Transactions on Magnetics International Magnetics Conference; 4–8 April 2005; Nagoya, Japan. New York, NY, USA: IEEE. pp. 3991-3993.

[7] Orlando B. Conception, réalisation et analyse de micro-inductances intégrées avec matériaux ferromagnétiques doux. applications aux inductances pour la conversion de puissance continue-continue et aux inductances variables MEMS pour circuits micro-ondes reconfigureurables. Université de Limoges, Limoges France, 2007 (article in French).

[8] Hsu HM. Investigation on the layout parameters of on-chip inductor. Microelectron Eng 2005; 37: 800-803.

[9] Peng AS, Chen KM, Huang GW, Wang SC, Chen HY, Chang CY. Characterization and modeling of silicon tapered inductors. In: NSTI 2004 Nanotechnology Conference and Trade Show; 7–11 March 2004; Boston, Massachusetts, USA. Austin, TX, USA: NSTI. pp. 155-158.

[10] Deleage O. Conception, réalisation et mise en œuvre d'un micro-convertisseur intégré pour la conversion DC/DC. Grenoble, France: Université de Joseph-Fourier, 2009.

[11] Chen J, Liou JJ. On-chip spiral inductors for RF applications. J Semicond Tech Sci 2004; 4: 149-167.

[12] Bechir MH, Yaya DD, Allassem D, Youssouf MK, Capraro S, Chatelon JP, Siblini A, Rousseau JJ. Inductances planaires intégrées à couches magnétiques: conception-fabrication-caractérisation-modélisation. In: 2014 Symposium De Génie Electrique; 8–10 July 2014; Cachan, France. Paris, France: EPF (Article in French).

[13] Zhang Y, Goplen B, Sapatnekar SS. Electrothermal analysis and optimization techniques for nanoscale integrated circuits. In: IEEE 2006 Electrical and Computer Engineering Conference; 24–27 January 2006; Yokohama, Japan. New York, NY, USA: IEEE. pp. 219-222.

[14] Yue CP, Wong SS. Physical modeling of spiral inductors on silicon. IEEE T Electron Dev 2000; 47: 560-568.

[15] Stojanović G, Zivanov L, Damnjanović M. Optimal design of circular inductors. Ser Elec Energ 2005; 18: 57-70.

[16] Meshkin R, Maghsoodi M, Saberkari A, Niaboli-Guilani M. High efficient CMOS class-E power amplifier with a new output power control scheme. J Elec Electron Eng Res 2013; 6: 77-82.

[17] Hershenson M, Mohan SS, Boyd SP, Lee TH. Optimization of inductor circuits via geometric programming. In: IEEE 1999 Design Automation Conference; 21–25 June 1999; New Orleans, LA, USA. New York, NY, USA: IEEE. pp. 994-998.

[18] Wang N, O'Donnell T, Roy S, McCloskey P, O'Mathuna C. Micro-inductors integrated on silicon for power supply on chip. J Magn Magn Mater 2007; 316: 233-237.

[19] Haddad E, Martin C, Joubert C, Allard B, Soueidan M. Modeling, fabrication, and characterization of planar inductors on YIG substrates. Adv Mat Res 2011; 324: 294-297.

[20] Haddad E, Christian M, Allard B, Soueidan M, Joubert C. Micro-fabrication of planar inductors for high frequency DC-DC power converters. In: Malkinski L, editor. Advanced Magnetic Materials. Rijeka, Croatia: InTechOpen, 2012. pp. 119-132.